Journal of Power Sources 194 (2009) 1202–1207

Contents lists available at ScienceDirect

Journal of Power Sources

journal homepage: www.elsevier.com/locate/jpowsour

Carbon nanotube/MnO_2 composites synthesized by microwave-assisted method for supercapacitors with high power and energy densities

Jun Yan [a], Zhuangjun Fan [a,*], Tong Wei [a], Jie Cheng [b], Bo Shao [a], Kai Wang [a], Liping Song [a], Milin Zhang [a]

[a] Key Laboratory of Superlight Materials and Surface Technology, Ministry of Education, College of Material Science and Chemical Engineering, Harbin Engineering University, Harbin 150001, PR China
[b] Research Institute of Chemical Defense, Beijing 100083, PR China

ARTICLE INFO

Article history:
Received 18 February 2009
Received in revised form 22 May 2009
Accepted 4 June 2009
Available online 11 June 2009

Keywords:
Manganese oxide
Microwave irradiation
Electrochemical properties

ABSTRACT

Carbon nanotube (CNT)/MnO_2 composites are synthesized by reduction of potassium permanganate under microwave irradiation. The morphology and microstructure of samples are examined by scanning electron microscopy (SEM), transition electron microscopy (TEM), X-ray diffraction (XRD) and X-ray photoelectron spectroscopy (XPS). Electrochemical properties are characterized by cyclic voltammetry (CV), galvanostatic charge/discharge and electrochemical impedance spectroscopy (EIS). Birnessite-type MnO_2 homogeneously coats on the surfaces of CNTs. For CNT–15%MnO_2 composite, the specific capacitance based on MnO_2 is 944 (85% of the theoretical capacitance) and 522 F g^{-1} at 1 and 500 mV s^{-1}, respectively. When the content of MnO_2 reaches 57 wt%, the composites have the maximum power density (45.4 kW kg^{-1}, the energy density is 25.2 Wh kg^{-1}). Therefore, CNT/MnO_2 composites prepared by microwave irradiation are promising electrode materials in hybrid vehicle systems.

1. Introduction

Supercapacitors, also called electrochemical capacitors (ECs) or ultracapacitors, have attracted considerable attention over the past decades because of their higher power density and longer cycle life than secondary batteries and their higher energy density compared to conventional electrical double-layer capacitors [1–6]. To develop an advanced supercapacitor device, an active electrode material with high capacity performance is indispensable [2,7]. From the materials point of view, porous carbon materials, conducting polymers, and transition-metal oxides are fundamental candidates used as supercapacitor electrode materials [1,3,8]. Each kind of material has its own advantages and disadvantages. Porous carbon materials have long cycle life and good mechanical properties, but low specific capacitance [8]. Conducting polymers are famous for their high flexibility, but have poor cyclability [9,10]. As for the transition-metal oxides, over the past decades, manganese oxides have received considerable attention for supercapacitors due to its low cost, abundance, high theoretical specific capacitance (~1100 F g^{-1}) and good environmental compatibility [5,11–15]. Zolfaghari et al. prepared nanostructured MnO_2 by a sonochemical method from an aqueous solution of potassium bromate and manganese sulfate and the maximum specific capacitance was 344 F g^{-1} at a scan rate of 5 mV s^{-1} in 0.5 mol L^{-1} Na_2SO_4 aqueous solution [16]. Ko et al. synthesized MnO_2/actived carbon nanotube (CNT) composite by the coprecipitation method and the specific capacitance was 250 F g^{-1} at a scan rate of 10 mV s^{-1} in 1 mol L^{-1} Na_2SO_4 aqueous solution [17]. Whereas, the specific capacitance of these oxides is only one-fifth or one-fourth of the theoretical value due to the limited charge transfer reaction kinetics resulted from the intrinsically poor electronic conductivity and difficulty in the penetration of electrolyte into the bulk of the oxide materials caused by the dense morphology [18]. Fan et al. have reported that the γ-MnO_2/CNT arrays was prepared by electrochemically induced deposition method and the specific capacitance was as high as 784 F g^{-1} based on γ-MnO_2 [19]. However, this thin film exhibited an unacceptable energy density values. In addition, the relatively high resistance of the oxide reduced seriously the current respond speed when the film was made thicker to increase the total charge/energy storage capacity, since only the surface film took part in the charge storage process [18]. Recently, Ma et al. have reported that the MnO_2/CNT nanocomposite prepared by a spontaneous direct redox reaction between CNTs and permanganate ions had the specific capacitance as high as 580 F g^{-1} based on MnO_2 [12]. However, such method was a complicated and time/energy-consuming process.

As a quick, simple, uniform and energy efficient heating method, microwave irradiation has been widely used in the industry and academia to synthesize such materials as porous materials [20,21], inorganic complex [22,23], nanocrystalline particles [24,25] and organic compounds [26]. In this paper, microwave irradiation was

* Corresponding author. Tel.: +86 451 82569890; fax: +86 451 82569890.
E-mail address: fanzhj666@163.com (Z. Fan).

0378-7753/$ – see front matter © 2009 Elsevier B.V. All rights reserved.
doi:10.1016/j.jpowsour.2009.06.006

Table 1
The amount of $KMnO_4$ added into CNT suspension and percentage of MnO_2 in the resulting CNT/MnO_2 composites.

Sample	Amount of $KMnO_4$ added into CNT suspension (g)	Mass percentage of MnO_2 in the composites (%)
CNT–15%MnO_2	0.0505	15
CNT–48%MnO_2	0.4741	48
CNT–57%MnO_2	1.8964	57

employed to synthesize CNT/MnO_2 composites by reduction of potassium permanganate with CNTs, and the electrochemical performance of CNT/MnO_2 composites was investigated, especially at high charge/discharge rates.

2. Experimental

2.1. Synthesis of CNT/MnO_2 composites

CNTs (multi-walled CNTs, Shenzhen Nanotech Port) were refluxed in 10 wt% nitric acid for 30 min to remove the catalyst particles and other impurities before use. All the other chemicals were of analytical grade and were used without further purification. The synthesis of CNT/MnO_2 composites was carried out as follows. First, 0.1575 g purified CNTs were dispersed in 100 mL distilled water by ultrasonic vibration for 6 h. Then predetermined amount of $KMnO_4$ as shown in Table 1 was added into the above suspension, and stirred for 1 h so that $KMnO_4$ could sufficiently absorb on the wall of CNTs. Subsequently, the mixture was heated using a household microwave oven (Haier MA-2270, 2450 MHz, 700 W). The reaction was carried out for 10 min, and then cooled to room temperature naturally. Finally, the suspension was filtered, washed several times with distilled water and absolute alcohol, and dried at 100 °C for 12 h in a vacuum oven. The resulting black powders were collected for the following characterization.

2.2. Characterization methods

The crystallographic structures of the materials were determined by a powder X-ray diffraction system (XRD, TTR-III) equipped with Cu Kα radiation (λ = 0.15406 nm). The microstructure of the samples was investigated by a scanning electron microscopy (SEM, Camscan Mx2600FE) and transition electron microscopy (TEM, JEOL JEM2000FX). Chemical state analysis was carried out by X-ray photoelectron spectroscopy (XPS) using a Kratos AXIS Ultra X-ray photoelectron spectrometer. A monochromatic Al source, operating at 210 W with a pass energy of 20 eV and a step of 0.1 eV, was utilized. All XPS spectra were corrected using the C 1s line at 284.6 eV. Curve fitting and background subtraction were accomplished using Casa XPS version 2.3.13 software. The mass percentage of MnO_2 in the composites was determined by dissolving the composites in 2 mol L^{-1} HNO_3 and using inductively coupled plasma-atomic emission spectroscopy (ICP-AES, Shimadzu ICPS-7500). In the following discussion, samples are labeled CNT–xMnO_2, where *x* is the mass percentage of MnO_2 calculated from the data of ICP-AES. The percentage of MnO_2 in the resulting CNT/MnO_2 composites is listed in Table 1.

2.3. Preparation of electrodes and electrochemical measurement

The fabrication of working electrodes was carried out as described elsewhere [27]. Briefly, the as-prepared composites, carbon black and poly(tetrafluoroethylene) (PTFE) were mixed in a mass ratio of 75:20:5 and dispersed in ethanol. Then the resulting mixture was coated onto the nickel foam substrate (1 cm × 1 cm) with a spatula, which was followed by drying at 100 °C for 12 h in a vacuum oven.

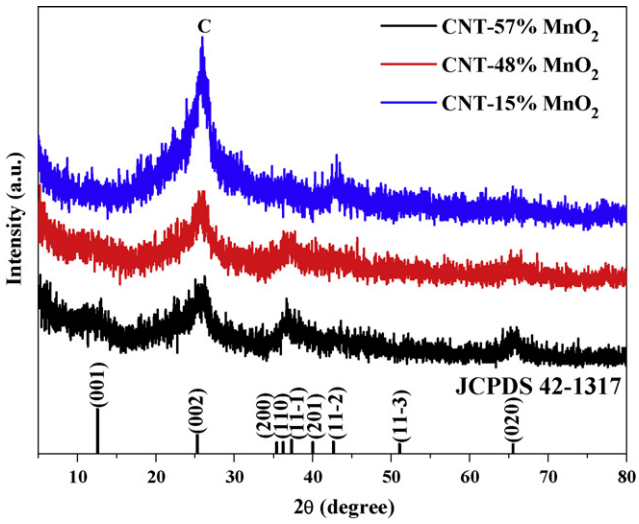

Fig. 1. Typical XRD patterns of the as-prepared CNT/MnO_2 samples.

All electrochemical measurements were done in a three-electrode setup: A Ni foam coated with CNT/MnO_2 composites as the working electrode, a platinum foil as the counter electrode, and a saturated calomel electrode (SCE) as the reference electrode. The measurements were carried out in a 1 mol L^{-1} Na_2SO_4 aqueous electrolyte at room temperature. Cyclic voltammetry (CV), galvanostatic charge/discharge and electrochemical impedance spectroscopy (EIS) were measured by a CHI 660C electrochemical workstation. CV tests were done between −0.1 and 0.9 V (vs. SCE) at different scan rates of 1, 2, 10, 20, 50, 100, 200 and 500 mV s^{-1}. Galvanostatic charge/discharge curves were measured at different current densities of 2, 10, 20 and 50 mA cm^{-2}, and EIS measurements were also carried out in the frequency range from 100 kHz to 0.1 Hz at open circuit potential with an ac perturbation of 5 mV.

3. Results and discussion

3.1. Microstructure characterizations

Fig. 1 shows the typical XRD patterns of the as-prepared CNT/MnO_2 samples. XRD analysis confirms the presence of carbon and birnessite-type MnO_2 (JCPDS 42-1317) with mixed crystalline and amorphous parts. Three broad peaks at 2θ around 12°, 37° and 66° can be indexed to birnessite-type MnO_2 [28,29]. The surface information of CNT/MnO_2 composites was collected by XPS. The peaks of Mn ($2p_{3/2}$, $2p_{1/2}$), O 1s and C 1s can be observed in the survey spectrum (Fig. 2(a)). The Mn $2p_{3/2}$ peak is centered at 642.1 eV and Mn $2p_{1/2}$ peak at 653.8 eV, with a spin-energy separation of 11.7 eV (Fig. 2(b)), which is in good agreement with the reported data of Mn $2p_{3/2}$ and Mn $2p_{1/2}$ in MnO_2 [30]. And this result is consistent with XRD analysis as mentioned above.

Fig. 3 shows the SEM and TEM images of the purified CNTs and the as-prepared CNT–57%MnO_2 composite. It can be seen that the purified CNTs exhibit regular morphology with the diameter of 20 nm and the wall is smooth, as shown in Fig. 3(a). The acid treatment modifies the CNTs with carbonyl, carboxyl and/or hydroxyl groups, which, together with the tube ends, are more reactive than the defect-free graphene surface of the CNTs, and hence more vulnerable to oxidation [29]. It is these defects that initiate the reaction between carbon and $KMnO_4$, and MnO_2 can be rapidly nucleated on the wall of CNTs under microwave irradiation. In a pH neutral

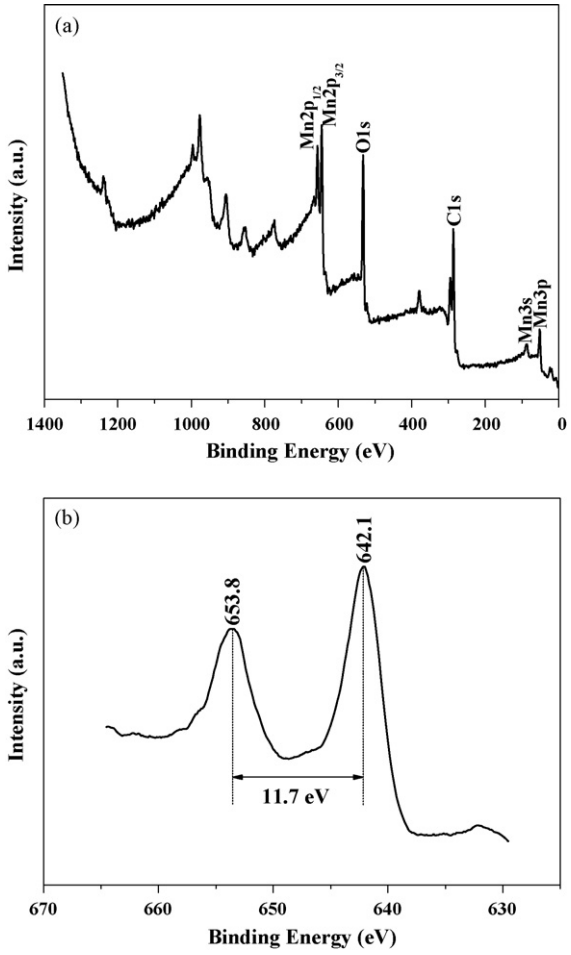

Fig. 2. (a) XPS survey spectra and (b) the magnification of Mn 2p region of the as-prepared CNT/MnO_2 composites.

solution, the reaction between carbon and $KMnO_4$ is as follows [29]:

$$4KMnO_4 + 3C + H_2O \rightarrow 4MnO_2 + K_2CO_3 + 2KHCO_3 \quad (1)$$

The above reaction is featured by electron transfer from the carbon to MnO_4^- upon direct contact so that a thin and homogenous MnO_2 coating is directly formed on the conductive CNT surface. This reaction can be remarkably promoted by microwave irradiation, and the reaction time (10 min) is much shorter than that of the previous reports (usually several hours under reflux or several days under ambient temperature) [28,29,31]. Once the available surfaces of CNTs are fully covered by MnO_2, the reaction is terminated. After MnO_2 deposition, the diameter of the CNTs increases slightly from 20 to 30 nm, as shown in Fig. 3(b, c), so the MnO_2 layer is about 5 nm in thickness. Besides, the surfaces of the CNTs become rougher than before (Fig. 3(b, c)), which indicates that the CNTs act as a substrate for the heterogeneous precipitation of a very thin layer of MnO_2 (Fig. 3(b)).

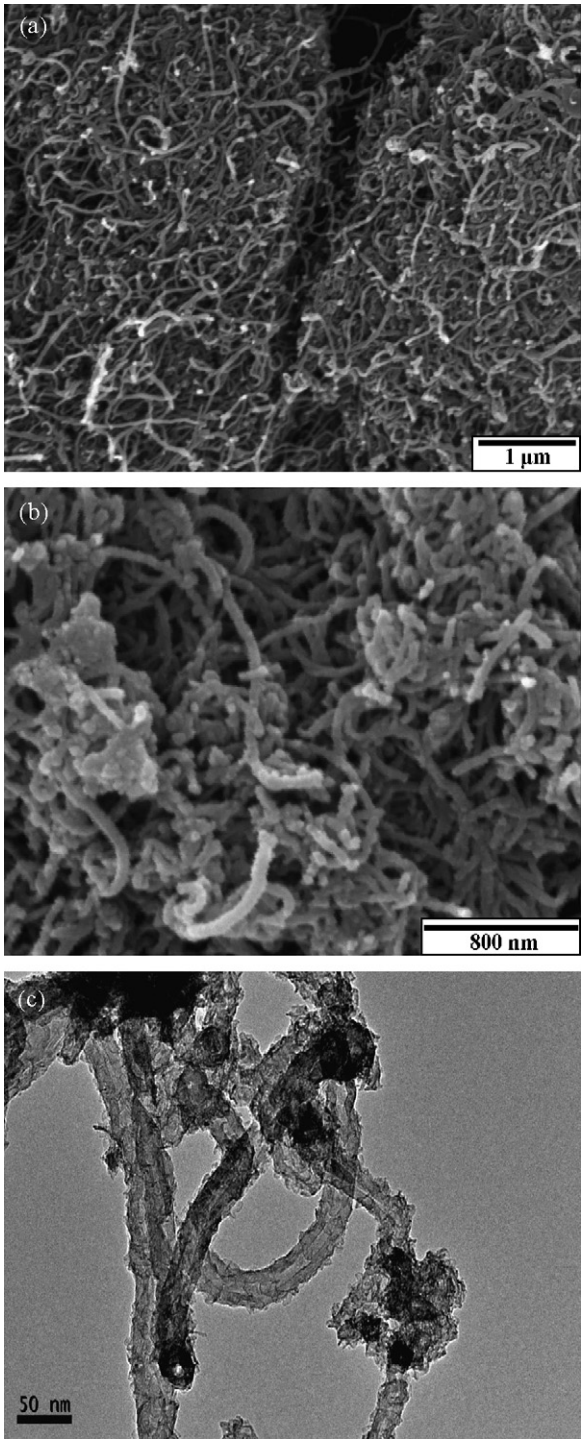

Fig. 3. SEM images of (a) purified CNTs and (b) CNT–57%MnO_2 composite. (c) TEM image of as-prepared CNT–57%MnO_2 composite.

3.2. Electrochemical behavior

The specific capacitance of the electrode can be calculated according to the following equation [31]:

$$C = \frac{1}{\omega\nu(V_c - V_a)} \int_{V_a}^{V_c} I(V)dV \quad (2)$$

where C is the specific capacitance ($F\,g^{-1}$), ω is the mass of the MnO_2 in the electrodes (g), ν is the potential scan rate ($mV\,s^{-1}$), $V_c - V_a$ is the sweep potential range during discharging (V) and $I(V)$ denotes the response current density ($A\,cm^{-2}$).

The variation in the specific capacitance of the CNT/MnO_2 composites as a function of the scan rates is plotted in Fig. 4. As shown, the specific capacitance decreases with the increasing amount of $KMnO_4$ at the same scan rate. For the CNT–15%MnO_2 sample, the initial specific capacitance based on MnO_2 is 944 (85% of the theoretical capacitance) and 522 $F\,g^{-1}$ at 1 and 500 $mV\,s^{-1}$, respectively, which is much higher than that of the other two samples. High content of CNTs in the composites can increase the effective contact

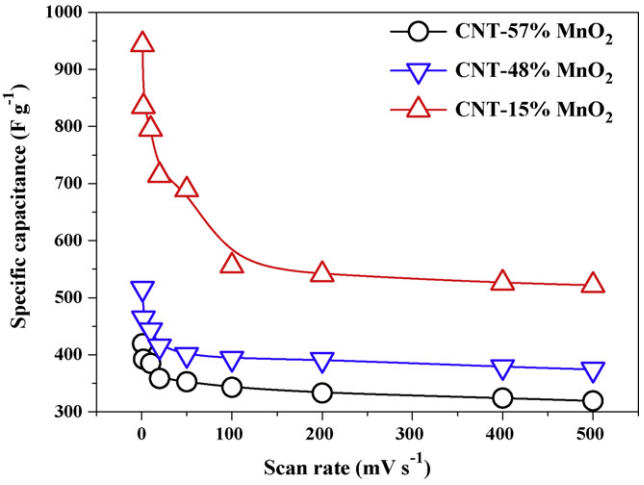

Fig. 4. Specific capacitance of CNT/MnO_2 composites based on MnO_2 at different scan rates.

area between MnO_2 and CNTs, which results in high electrochemical utilization of MnO_2 in the CNT/MnO_2 composites. At the same time, CNTs can provide a direct conductive path for MnO_2 particles due to their high electric conductivity, thus reducing the internal resistance within the composite itself. Furthermore, the inter-tube pores among CNTs facilitate the rapid transport of the electrolyte ions from bulk solution to the surface of MnO_2.

In order to further understand the high electrochemical utilization of MnO_2 for CNT–15%MnO_2 composite, voltammetric charges (q) have been determined as a function of scan rates (ν) [31–33]. The dependences of q on $\nu^{-1/2}$ and q^{-1} on $\nu^{1/2}$ are shown in Fig. 5. In the case of a reversible redox transition, the dependence of q on ν is usually explained by the slow diffusion of protons into pores, cracks, and grains boundaries [33,34]. At a high scan rate, diffusion limitation slows the accessibility of protons to the inner surface of the electrode material. The electrochemical response then depends only on the outer active surface, which is straightforwardly accessible to protons. The extrapolation of q to $\nu = \infty$ from the q vs. $\nu^{-1/2}$ plot (Fig. 5(a)) gives the outer charge (q_0), which is related to the outer and more accessible active surface. At a low scan rate, protons have enough time to diffuse to the inner and less accessible active surface. The extrapolation of q to $\nu = 0$ from the q^{-1} vs. $\nu^{1/2}$ (Fig. 5(b)) gives the total charge (q_T), which is related to the whole active surface including the outer and inner active surface [32,33].

The estimated charge density ($C\,g^{-1}$) at very low and very high scan rates for CNT–15%MnO_2 sample is presented in Table 2. It can be seen that the charge of CNT–15%MnO_2 sample at very low scan rate is $1050\,C\,g^{-1}$, which is very close to the theoretical value ($\sim 1100\,C\,g^{-1}$). This is primarily attributed to high electrical conductivity of the composite and homogenous dispersion of MnO_2 on the surfaces of CNTs, facilitating the rapid transport of the electrolyte ions and increasing the electrochemical utilization of MnO_2. At very high scan rate, the outer charge reached a limit of $550\,C\,g^{-1}$, indicating that only 52.4% of the manganese surface atoms participate in the Faradaic process. One explanation can be that such a high rate limits the diffusion of Na^+ ions and/or protons throughout the whole volume of the electrode and consequently some pores and voids remain inaccessible at high sweep rates. At $1\,mV\,s^{-1}$, the ratio

Table 2
The estimated charge density at very low and very high scan rates, and q_0/q_T, q_r/q_T (q_r at $1\,mV\,s^{-1}$) for CNT–15%MnO_2 sample.

Sample	q_0 ($C\,g^{-1}$)	q_T ($C\,g^{-1}$)	q_r ($C\,g^{-1}$)	q_0/q_T (%)	q_r/q_T (%)
CNT–15%MnO_2	550	1050	944	52.4	89.9

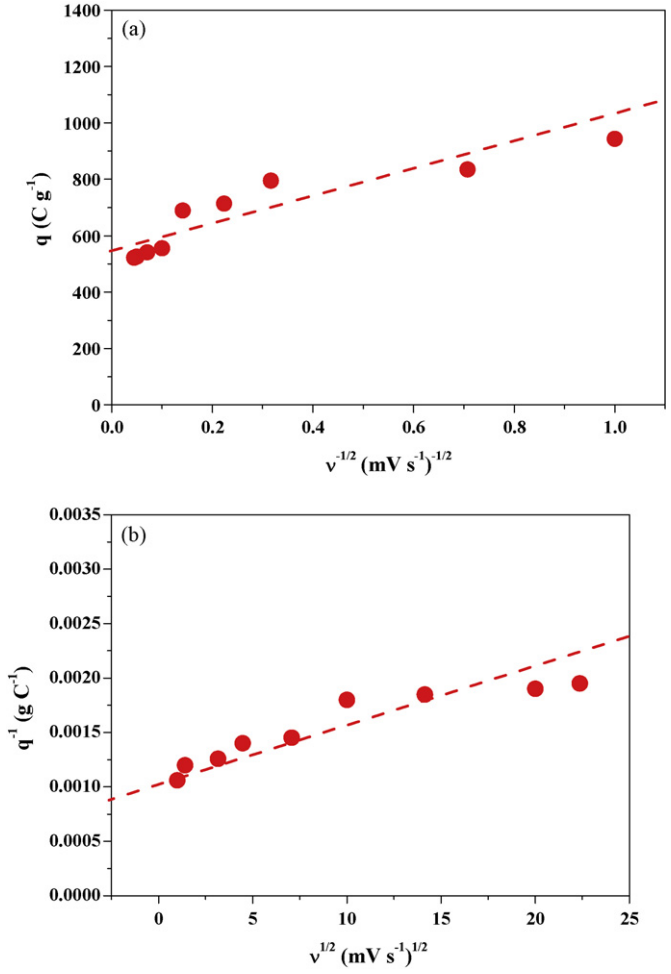

Fig. 5. Variation of the voltammetric charge density (q) with respect to scan rates (ν): (a) extrapolation of q to $\nu = \infty$ from the q vs. $\nu^{-1/2}$ plot given the outer charge and (b) extrapolation of q to $\nu = 0$ from the q^{-1} vs. $\nu^{1/2}$ plot given the total charge for CNT–15%MnO_2 composite.

of real charge (q_r) to q_T (89.9%, Table 2) may symbolize the utilization of MnO_2 involved in the charge storage process, indicating the higher electrochemical utilization of MnO_2.

The CV curves at different scan rates from 1 to $500\,mV\,s^{-1}$ of CNT–15%MnO_2 composite are shown in Fig. 6. These CV curves are relatively rectangular in shape without obvious redox peaks, indicating that CNT–15%MnO_2 has ideal capacitive behavior. No obvious distortion in the CV curves is observed as the potential scan rate is increased, even at a very high scan rate of $500\,mV\,s^{-1}$, the CV curve still retain the rectangular shape (Fig. 6(b)). The excellent CV shape at such a high scan rate reveals a very rapid current response on voltage reversal at each end potential. Meanwhile, the straight rectangular sides represent a very small equivalent series resistance (ESR) of the electrode and also the fast diffusion of electrolyte ions in the composite.

The long-term cycle stability of the CNT–15%MnO_2 composite was also evaluated in this study by repeating the CV test between −0.1 and 0.9 V (vs. SCE) at a scan rate of $20\,mV\,s^{-1}$ for 500 cycles. The specific capacitance based on MnO_2 as a function of cycle number is presented in Fig. 7. The electrode is found to exhibit excellent stability over the entire cycle numbers. After 500 cycles, the capacitance decreases only 5.4% of initial capacitance demonstrating a great cycle stability. The decrease of specific capacitance could be attributed to the partial dissolution of MnO_2 by the formation of soluble Mn^{2+} ions [18].

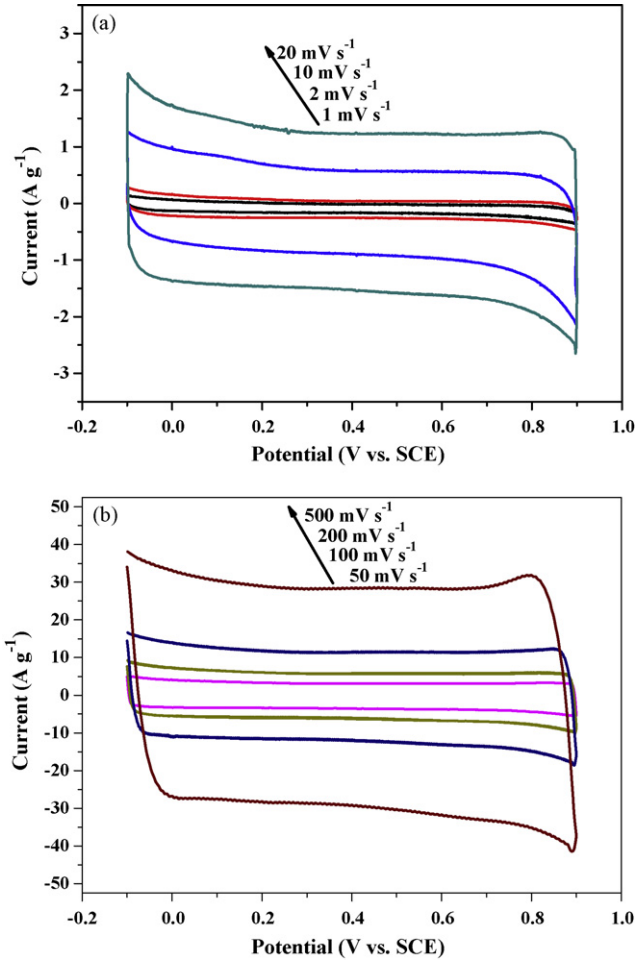

Fig. 6. CV curves of CNT–15%MnO_2 composite at different scan rates of (a) 1, 2, 10, 20, (b) 50, 100, 200 and 500 mV s^{-1}.

Impedance of the CNT–15%MnO_2 after 1st and 500th cycle were measured in the frequency range of 100 kHz–0.1 Hz at open circuit potential with an ac perturbation of 5 mV (Fig. 8). It could be obviously seen that the impedance spectra are almost similar in form, composed of one semicircle at high-frequency end followed by a linear part at the low-frequency end. Both the spectra show nearly 90° capacitive spike starting from the mid-high frequency, indicating the suitability of the CNT–15%MnO_2 composite as an electrode material for supercapacitors. However, an obvious difference between the two spectra is, after 500 cycles, the pseudo-charge transfer resistance (R_{ct}) has increased from 0.14 to 0.77 Ω (Fig. 8), which is probably attributed to the loss of adhesion of some active material with the current collector or the dissolution of some MnO_2 [18].

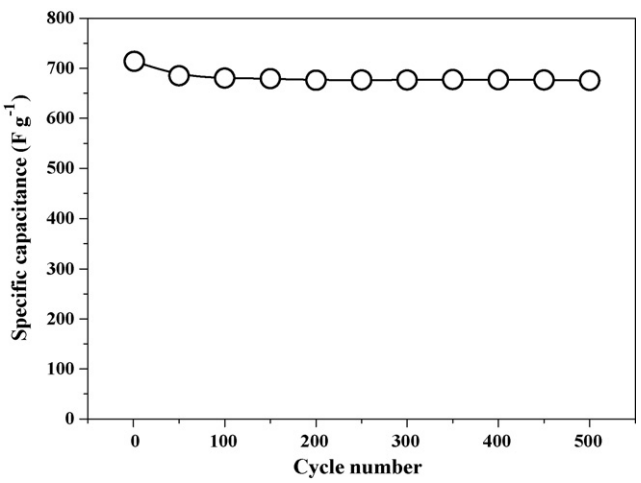

Fig. 7. Variation of the specific capacitance of CNT–15%MnO_2 electrode as a function of cycle number measured at 20 mV s^{-1} in 1 mol L^{-1} Na_2SO_4 aqueous solution.

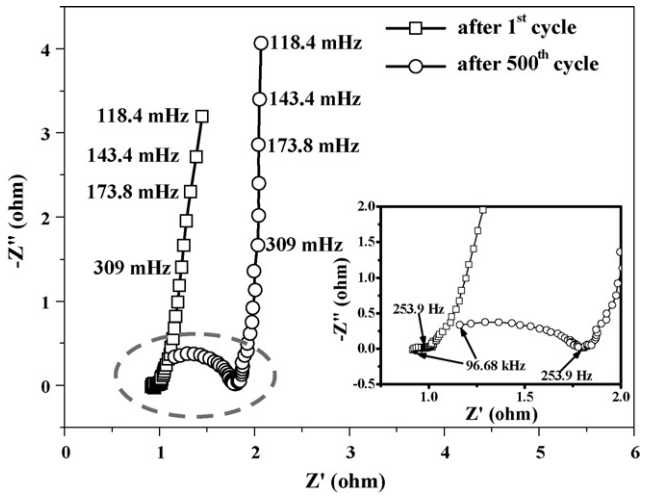

Fig. 8. Nyquist plots of CNT–15%MnO_2 electrode in the frequency range of 100 kHz to 0.1 Hz measured during the cycle life testing (inset is the enlargement of dashed segment, representing the high-frequency region).

Power density and energy density, as important parameters for the investigation of the electrochemical performance of electrochemical cells, have been also used to characterize the as-prepared materials [16,35]. The power density and the energy density can be estimated from the following equations [16]:

$$E = \frac{1}{2}C(\Delta V)^2 \quad (3)$$

$$P = \frac{Q\,\Delta V}{2t} = \frac{E}{t} \quad (4)$$

where P, C, Q, ΔV, t and E are indicating of the average power density (W kg^{-1}), specific capacitance based on the mass of the electroactive material (F g^{-1}), total charge delivered (C), the potential window of discharge (V), discharge time (s) and average energy density (Wh kg^{-1}), respectively. Ragone plot of CNT–57%MnO_2

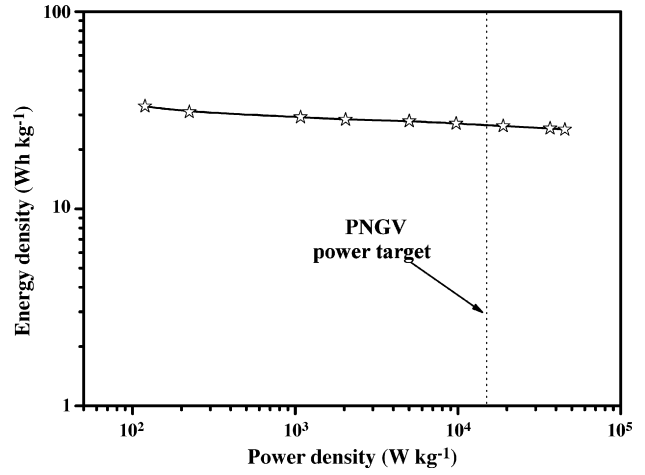

Fig. 9. Ragone plot of CNT–57%MnO_2 electrode in 1 mol L^{-1} Na_2SO_4 solution (the PNGV power target (15 kW kg^{-1}, in terms of electroactive material weight) is also shown).

composite at different scan rates is shown in Fig. 9. The energy densities reduce slowly with increasing power densities. The energy density of CNT-57%MnO_2 composite can reach 33.1 Wh kg^{-1} at a power density of 119.3 W kg^{-1}, and still remains 25.2 Wh kg^{-1} at a power density of 45.4 kW kg^{-1}. More importantly, the power density measured for CNT–57%MnO_2 can reach the power target of the Partnership for a New Generation of Vehicles (PNGV, 15 kW kg^{-1}) [10], suggesting that such composite is a promising electrode material for component in hybrid vehicle systems.

4. Conclusions

In this paper, CNT/MnO_2 composites have been synthesized by reduction of potassium permanganate under microwave irradiation. For CNT–15%MnO_2 composite, the specific capacitance based on MnO_2 is 944 (85% of the theoretical capacitance) and 522 F g^{-1} at 1 and 500 mV s^{-1}, respectively. The composite also show excellent cycle stability, and the capacitance decreases only 5.4% after 500 cycles. The excellent capacitive performance is primarily attributed to high electrical conductivity of the composites and homogenous dispersion of MnO_2 on the surfaces of CNTs, facilitating the rapid transport of the electrolyte ions and increasing the electrochemical utilization of MnO_2. For CNT–57%MnO_2 composite, the maximum power density is 45.4 kW kg^{-1}(energy density is 25.2 Wh kg^{-1}). Therefore, the CNT/MnO_2 composites prepared by microwave irradiation are very suitable and promising electrode materials for supercapacitors with high power and energy densities.

Acknowledgements

This work was supported by the Key Project of Chinese Ministry of Education (No. 106011), Foundation of Harbin Innovation Fellow (2006RFQXG030, 2007RFQXG028) and Fundamental Research Foundation of Harbin Engineering University (Project HEUFT07094).

References

[1] B.E. Conway, Electrochemical Supercapacitors: Scientific Fundamentals and Technological Applications, Kluwer Academic/Plenum Publishers, New York, 1999.
[2] G.-W. Yang, C.-L. Xu, H.-L. Li, Chem. Commun. 48 (2008) 6537.
[3] P. Simon, Y. Gogotsi, Nat. Mater. 7 (2008) 845.
[4] J.-K. Chang, C.-H. Huang, W.-T. Tsai, M.-J. Deng, I.W. Sun, J. Power Sources 179 (2008) 435.
[5] G. An, P. Yu, M. Xiao, Z. Liu, Z. Miao, K. Ding, L. Mao, Nanotechnology 19 (2008) 275709.
[6] D. Liu, Q. Zhang, P. Xiao, B.B. Garcia, Q. Guo, R. Champion, G. Cao, Chem. Mater. 20 (2008) 1376.
[7] C.-C. Hu, K.-H. Chang, M.-C. Lin, Y.-T. Wu, Nano Lett. 6 (2006) 2690.
[8] S.-L. Chou, J.-Z. Wang, S.-Y. Chew, H.-K. Liu, S.-X. Dou, Electrochem. Commun. 10 (2008) 1724.
[9] D.-W. Wang, F. Li, Z.-G. Chen, G.Q. Lu, H.-M. Cheng, Chem. Mater. 20 (2008) 7195.
[10] D.W. Wang, F. Li, M. Liu, G.Q. Lu, H.M. Cheng, Angew. Chem. Int. Ed. 47 (2008) 373.
[11] J.K. Chang, S.H. Hsu, W.T. Tsai, I.W. Sun, J. Power Sources 177 (2008) 676.
[12] S.B. Ma, K.W. Nam, W.S. Yoon, X.Q. Yang, K.Y. Ahn, K.H. Oh, K.B. Kim, J. Power Sources 178 (2008) 483.
[13] S. Komaba, A. Ogata, T. Tsuchikawa, Electrochem. Commun. 10 (2008) 1435.
[14] E. Beaudrouet, A. Le Gal La Salle, D. Guyomard, Electrochim. Acta 54 (2009) 1240.
[15] X. Zhang, W. Yang, D.G. Evans, J. Power Sources 184 (2008) 695.
[16] A. Zolfaghari, F. Ataherian, M. Ghaemi, A. Gholami, Electrochim. Acta 52 (2007) 2806.
[17] J.M. Ko, K.M. Kim, Mater. Chem. Phys. 114 (2009) 837.
[18] S.R. Sivakkumar, J.M. Ko, D.Y. Kim, B.C. Kim, G.G. Wallace, Electrochim. Acta 52 (2007) 7377.
[19] Z. Fan, J. Chen, B. Zhang, B. Liu, X. Zhong, Y. Kuang, Diam. Relat. Mater. 17 (2008) 1943.
[20] G.A. Tompsett, W.C. Conner, K.S. Yngvesson, Chemphyschem 7 (2006) 296.
[21] H.I. Lee, J.H. Kim, S.H. Joo, H. Chang, D. Seung, O.-S. Joo, D.J. Suh, W.-S. Ahn, C. Pak, J.M. Kim, Carbon 45 (2007) 2851.
[22] J.-F. Zhu, Y.-J. Zhu, J. Phys. Chem. B 110 (2006) 8593.
[23] M. Wu, L. Zhang, D. Wang, J. Gao, S. Zhang, Nanotechnology 18 (2007) 385603.
[24] Y. Wang, Z. Iqbal, S. Mitra, Carbon 44 (2006) 2804.
[25] S. Komarneni, D. Li, B. Newalkar, H. Katsuki, A.S. Bhalla, Langmuir 18 (2002) 5959.
[26] Z. An, W. Tang, C.J. Hawker, G.D. Stucky, J. Am. Chem. Soc. 128 (2006) 15054.
[27] J. Yan, Z. Fan, T. Wei, Z. Qie, S. Wang, M. Zhang, Mater. Sci. Eng. B 151 (2008) 174.
[28] S.B. Ma, K.Y. Ahn, E.S. Lee, K.H. Oh, K.B. Kim, Carbon 45 (2007) 375.
[29] X. Jin, W. Zhou, S. Zhang, G.Z. Chen, Small 3 (2007) 1513.
[30] C.D. Wanger, W.M. Riggs, L.E. Davis, J.F. Moulder, G.E. Muilenberg, Handbook of X-ray Photoelectron Spectroscopy, Perkin-Elmer, Eden Prairie, 1978.
[31] X.F. Xie, L. Gao, Carbon 45 (2007) 2365.
[32] S. Ardizzone, G. Fregonara, S. Trasatti, Electrochim. Acta 35 (1990) 263.
[33] C.J. Xu, B.H. Li, H.D. Du, F.Y. Kang, Y.Q. Zeng, J. Power Sources 180 (2008) 664.
[34] P. Soudan, J. Gaudet, D. Guay, D. Bélanger, R. Schulz, Chem. Mater. 14 (2002) 1210.
[35] T. Shinomiya, V. Gupta, N. Miura, Electrochim. Acta 51 (2006) 4412.